

# Scalable Quickest Line Outage Detection and Localization Via Graph Spectral Analysis

Anmol Dwivedi and Ali Tajer<sup>✉</sup>, Senior Member, IEEE

**Abstract**—This paper proposes a *scalable* framework for the *real-time* detection and localization of power line outages in transmission networks. While localizing outages is pivotal for ensuring grid reliability, forming such decisions faces an inherent combinatorial complexity that grows with the grid size and becomes prohibitive even for moderate grid sizes. Hence, designing outage detection and localization algorithms that are amenable to real-time implementation critically hinges on circumventing the computational complexity. This paper proposes a graph-guided quickest change detection (GG-QCD) approach that leverages the grid topology and performs quickest change detection in the spectral domain of the graph underlying grid's topology. The GG-QCD algorithm's key features are that (i) it uses a one-dimensional metric that tests the data's conformity to the grid topology, and (ii) it decouples the detection and localization processes to avoid testing all the lines at all times. Specifically, a lack of such conformity of the data to the system model will be alarming the potential existence of an outage. Once an outage is deemed to exist, an active graph clustering approach will be used to localize the line in outage. The clustering approach will also be relying on the same one-dimensional conformity metric. Overall, this approach will be performing *only one* test over time when the system is outage-free. Once an outage is detected, it will require  $\mathcal{O}(\log(L))$  additional tests to identify the line in outage. This paper presents the theory for GG-QCD and algorithms for outage detection and localization. To evaluate these algorithms' efficiency and complexity, they are examined in the standard IEEE 30- and 118-bus systems.

**Index Terms**—Graph spectrum, outage detection, quickest detection, scalable.

## I. INTRODUCTION

VARIOUS monitoring (e.g., reliability and safety), inferential (e.g., state estimation), and decision-making (e.g., power flow optimization) in power systems critically hinge on accurate and real-time awareness of the systems model (e.g., line parameters and topology). However, network models are prone to disruptions and variations induced by a wide range of failures or inaccurate telemetry in the system. As a result, the decisions predicated on an erroneous system model may lead to hidden failures that propagate and eventually result in large-scale

Manuscript received December 27, 2020; revised May 11, 2021; accepted June 26, 2021. Date of publication July 1, 2021; date of current version December 23, 2021. This work was supported in part by the U.S. National Science Foundation under the CAREER Award ECCS-1554482. Paper no. TPWRS-02116-2020. (*Corresponding author: Ali Tajer*)

The authors are with the Electrical, Computer, and Systems Engineering Department, Rensselaer Polytechnic Institute, Troy, NY 12180 USA (e-mail: dwivea2@rpi.edu; tajer@ecse.rpi.edu).

Color versions of one or more figures in this article are available at <https://doi.org/10.1109/TPWRS.2021.3094202>.

Digital Object Identifier 10.1109/TPWRS.2021.3094202

disruptions in monitoring, control, and planning. For instance, in a report by North American Electric Reliability Corporation, it was investigated and concluded that inadvertent tripping of a power line lead to a series of cascading failures causing a large-scale blackout in North America 2003 [1]. Therefore, real-time and accurate situation awareness about network models has a pivotal role in ensuring the reliability, stability, and efficiency of power distribution.

Line outage events constitute a major form of disruptive model change since they induce topology changes and force power redistribution. Such redistribution of power translates to potentially significant suboptimal power flows or even stressing more transmission lines and leading to more line outages. There exists a rich literature on leveraging statistical methods for agile and reliable detection and localization of outages as soon as they occur. Some studies relevant to the scope of this paper include the study in [2], [3], which proposes an exhaustive search algorithm to detect and localize single- and double-line outages. While accurate, such approaches face high computational complexities. For addressing the computational aspect, the study in [4] proposes modeling the collection of voltage phase angles over the grid by a Gauss-Markov random field (GMRF), and it formulates outage detection as an inference problem and employs hypothesis testing for outage detection. Following a similar graphical model approach, the studies in [5], [6] propose an adaptive strategy to detect and localize outages with the fewest number of measurements. Other approaches that exploit the network's structure include the study in [7] that assumes sparsity in the topology and develops a factor graph representation of the grid. This model is leveraged to employ efficient message-passing algorithms for outage detection. The study in [8] leverages the structure in the sparsity of anomalous events, and it formulates outage localization as a sparse signal reconstruction objective that is addressed by using compressive sensing for identifying multiple line outages. Along similar lines, the studies in [9] and [10] use optimization-based approaches, and the studies in [11] and [12] design data-driven algorithms that are trained offline and further employed for real-time topology identification. Outage identification has also been considered in power distribution systems where tree topological structures are exploited. Specifically, the study in [13] breaks down the combinatorial outage hypothesis space into smaller areas and propose computationally efficient algorithms for outage detection.

In another direction, close to this paper's scope, the quickest change detection (QCD) theory is applied to line outage detection in [14]–[16]. The QCD theory aims to detect abrupt

changes in the statistical model of time series data. Its objective is to detect the change-point with minimal delay after the change, while in parallel, the quality of the decisions (e.g., false alarm rates) are controlled [17]. In [14], a QCD algorithm is proposed for the quick detection and localization of line outages when the outages are persistent. These approaches generally use high-dimensional measured data (e.g., voltage phase angles of all buses in the network) and design a customized statistical test for each transmission line, based on the line's parameters. These possibly different tests are performed in parallel at all times to detect outages and localize the lines in outage, when the outages are persistent. The studies in [15] and [16] further extend these studies to address the transient dynamics of outage events. QCD algorithms for line outage detection in power distribution systems and fault detection in photovoltaic systems are investigated in [18] and [19], respectively. These classes of QCD algorithms rely on computing high-dimensional statistics, and we refer to them as high-dimensional QCD (HD-QCD) algorithms.

In this paper, we propose a *scalable* and *computationally tractable* QCD algorithm for detecting and localizing outages to address the computational challenges of the HD-QCD algorithms. To lay context for discussions, we note that the HD-QCD approaches face two critical computational challenges: (i) in a system with  $L$  lines, it requires performing  $L$  parallel tests at all times, and (ii) each of the tests involves computing an  $N$ -dimensional likelihood ratio, which has high complexity as  $N$  grows (see [20] for detailed discussions). The combination of these, for even moderate network sizes, renders the tests computationally prohibitive. In this paper, we propose to perform QCD in the spectral domain of the graphical model associated with the network's topology and refer to it as graph-guided QCD (GG-QCD). Specifically, due to the network structure (topology), the data generated (e.g., voltage phase angles) has an inherent structure that can be leveraged to test the data's conformity to the known network structure.

We specify metrics that quantify spectral change caused in the event of an outage, and subsequently, provide reliable metrics for testing the conformity of the data to the network model. Based on these metrics, we address the two computational complexities mentioned above. First, we note that detecting outages (a binary decision about whether an outage exists in the network) is far less computationally complex than line outage localization (an  $L$ -array decision). Motivated by this, we start with a detection stage and will not proceed to localization until there exists sufficient evidence that an outage has occurred. Such decoupling of detection and localization processes allows for only one test (as opposed to  $L$  parallel tests) when the network is outage-free, which is a significant fraction of the time. Furthermore, this test will be using a 1-dimensional conformity metric, which is significantly less complex than computing  $L$ -dimensional likelihood ratios. Once there is sufficient evidence that an outage has occurred, we initiate the localization stage. At its core, the localization procedure recursively partitions the topological network and concurrently employs conformity tests to progressively eliminate regions that are deemed to behave normally and retain the rest for more scrutiny until the line in

outage is localized. Inspired by the binary search algorithm, such strategies obviate the requirement to carry out parallel tests for each alternative outage possibility, reducing the order of statistical tests to at most  $\log L$ . Furthermore, similarly to the detection stage, each of these tests will involve computing 1-dimensional statistical metrics.

The rest of the paper is organized as follows. The system model and associated notations are presented in Section II. Section III formalizes the graph spectrum metrics, which are also used to formalize the outage detection and localization problems. Algorithms for line outage detection and localization are presented in Section IV and V, respectively. Section VI illustrates the performance of the proposed algorithm in the standard IEEE 30- and 118-bus systems, and Section VII concludes the paper.

## II. PRELIMINARIES AND NOTATION

### A. Power System Model

Consider a power system of  $N$  buses and  $L$  transmission lines connecting the buses. We represent this network by a weighted graph  $\mathcal{G} \triangleq (V, E, \mathbf{B})$ . The set of vertices  $V \triangleq \{1, \dots, N\}$  represent the buses. The edge set  $E \triangleq V \times V$  represents the transmission lines. There is an edge between vertices  $i, j \in V$ , denoted by  $E_{ij}$  if buses  $i$  and  $j$  are connected by a transmission line. Matrix  $\mathbf{B} \in \mathbb{R}^{N \times N}$  is the susceptance matrix, in which  $y_{ij} \triangleq [\mathbf{B}]_{ij}$  is the susceptance of the transmission line  $E_{ij}$ . Denote the Laplacian matrix associated with  $\mathbf{B}$  by  $\mathcal{L}_{\mathbf{B}}$ , where

$$[\mathcal{L}_{\mathbf{B}}]_{ij} \triangleq \begin{cases} \sum_{j \in \mathcal{N}_i} y_{i,j}, & \text{if } i = j \\ -y_{i,j}, & \text{if } (i, j) \in E \\ 0, & \text{otherwise} \end{cases} \quad (1)$$

and  $\mathcal{N}_i$  denotes the set of buses that are directly connected by a transmission line to bus  $i$ . We denote the voltage phase angle of bus  $i$  at time  $t$  by  $\theta_i(t)$  and accordingly, define  $\boldsymbol{\theta}(t) \triangleq [\theta_1(t), \dots, \theta_N(t)]^\top$ . Subsequently, we denote the injected real power at bus  $i$  by  $P_i(t)$ , which, in general, is a non-linear function of  $\boldsymbol{\theta}(t)$ . These measurements are sampled by a phasor measurement unit (PMU) regularly at  $\Delta t$  intervals (in seconds), rendering discrete-time measurements at discrete time instants  $\{n\Delta t : n \in \mathbb{N}\}$ . We denote the discrete time measurements associated with bus  $i \in V$  by  $\theta_i[n] \triangleq \theta_i(n\Delta t)$  and  $P_i[n] \triangleq P_i(n\Delta t)$ , and accordingly denote the variations in voltage phase angles and active power injections in bus  $i$  between consecutive sampling instances by  $\Delta\theta_i[n] \triangleq \theta_i[n+1] - \theta_i[n]$  and  $\Delta P_i[n] \triangleq P_i[n+1] - P_i[n]$ . We treat bus 1 as the reference bus, and its voltage phase angle serves as the system's phase reference. Under proper decoupling<sup>1</sup> and DC<sup>2</sup> assumptions we

<sup>1</sup>Variations in active power injections dominantly affect voltage angles and variations in reactive power injections primarily affect bus voltage magnitudes.

<sup>2</sup>(i) The system is lossless; (ii) voltage magnitudes are constant (1 per unit), and (iii) at any given time, voltage phase angles between neighboring buses are small, i.e.,  $|\theta_i[n] - \theta_j[n]| \ll 1$  for all  $i \neq j$  such that  $E_{ij} \in E$  and at all times  $n$ .

have the following linear relationships [14]:

$$\Delta P_i[n] \approx \sum_{j \in V, j \neq 1} [\mathcal{L}_B]_{ij} \cdot \Delta \theta_j[n] \quad \forall i \in V \setminus \{1\}. \quad (2)$$

More compactly, we define  $\Delta \theta[n] \triangleq [\Delta \theta_2[n], \dots, \Delta \theta_N[n]]$  and  $\Delta \mathbf{P}[n] \triangleq [\Delta P_2[n], \dots, \Delta P_N[n]]$ , yielding

$$\Delta \mathbf{P}[n] \approx \tilde{\mathcal{L}}_B \cdot \Delta \theta[n]. \quad (3)$$

where, matrix  $\tilde{\mathcal{L}}_B$  is constructed by removing the rows and columns associated with the reference bus in  $\mathcal{L}_B$ . Due to constant load fluctuations and changes in power flow dynamics, there exist small-scale temporal variations in  $\Delta \mathbf{P}[n]$ .

### B. Post-Outage Statistical Model

When a transmission line undergoes an outage, it induces a topological change, resulting in a change in  $\mathbf{B}$ . Specifically, when line  $E_{uv}$  undergoes an outage, the Laplacian matrix of  $\mathbf{B}_{uv}$ , denoted by  $\tilde{\mathcal{L}}_B^{uv}$ , is related to  $\tilde{\mathcal{L}}_B$  via the rank-one update:

$$\tilde{\mathcal{L}}_B^{uv} = \tilde{\mathcal{L}}_B - y_{uv} \cdot \mathbf{r}_{uv} \cdot \mathbf{r}_{uv}^\top \quad (4)$$

where  $\mathbf{r}_{uv} \in \mathbb{R}^{N-1}$  is an all-zero vector, with the excepts that its  $(u-1)^{\text{th}}$  entry is +1 and its  $(v-1)^{\text{th}}$  entry is -1. This renders the post-outage model

$$\Delta \mathbf{P}[n] \approx \tilde{\mathcal{L}}_B^{uv} \cdot \Delta \theta[n]. \quad (5)$$

These changes, impose abrupt changes in the statistical model associated with the vector  $\Delta \theta[n]$ . We define  $g_{uv}$  as the post-change probability density function (pdf) of  $\Delta \theta[n]$  when  $E_{uv}$  is in outage. Hence, when  $E_{uv}$  undergoes an outage at a random time  $\gamma$ , we have the following pre- and post-change statistical models

$$\begin{aligned} \text{pre-change: } \Delta \theta[n] &\sim g \quad \text{for } n < \gamma \\ \text{post-change: } \Delta \theta[n] &\sim g_{uv} \quad \text{for } n \geq \gamma. \end{aligned} \quad (6)$$

$\Delta \theta[n]$  is assumed to be temporally independent and identically distributed with joint pdf  $g : \mathbb{R}^N \rightarrow \mathbb{R}_+$ . This is owing to the small variations in real power injection  $\Delta \mathbf{P}[n]$  over short sampling time scales attributed to random fluctuations in electricity consumption and the subsequent response of some generators [14]. Hence, by leveraging (5), we find the statistical model of  $\Delta \theta[n]$ .

## III. GRAPH SPECTRAL ANALYSIS OF OUTAGES

### A. Motivation

Our objective is to detect and localize an outage with minimal delay after the outage occurs, while in parallel, the rate of false alarms is controlled to be confined below a pre-specified rate. A direct solution explored in [14] involves designing an exclusive test for each of the  $L$  transmission lines and running all the tests at all times in parallel. Such an approach faces three complexity challenges:

- C<sub>1</sub>: The number of tests required scales linearly with  $L$ .
- C<sub>2</sub>: All the tests run at all times. The reason is that this approach aims to perform outage localization at the same

time that an outage is detected. This, inevitably, requires constantly monitoring the individual line outage events.

- C<sub>3</sub>: Most importantly, the complexity of each test becomes prohibitive as  $L$  grows even beyond moderate values (since they involve computing the values of the  $N$ -dimensional joint pdfs).

We aim to design an approach with the following properties:

- P<sub>1</sub>: By decoupling the *detection* and *localization* tasks, we perform localization only after an outage is detected. Hence, we can avoid running all the  $L$  tests at all times and instead will run only one test until an outage is detected.
- P<sub>2</sub>: Furthermore, when the outage is detected, the number of tests required for localizing the line in outage scales with  $\mathcal{O}(\log_2(L))$ , as opposed to  $\mathcal{O}(L)$ .
- P<sub>3</sub>: Finally, each test becomes considerably less computationally complex (to be discussed in Section VI-A).

### B. Measuring Conformity of Data to Model

We use spectral graph theory to analyze the geometry of the collected data  $\Delta \theta[n]$  and its conformity to the system's inherent structure captured by the graphical model  $\mathcal{G}$ . We quantify conformity as the key measure for detection and localizing an outage. This is motivated by the following simple principle: when there is an outage in line  $E_{uv}$ , owing to the strong inter-connectivity in the system, it will likely render a geometric change in the data beyond simply the data generated by the PMUs of buses  $u$  and  $v$ . The data's geometry is partly captured by the spectrum of the graph  $\mathcal{G} \triangleq (V, E, \mathbf{B})$ . To formalize the framework, we start by defining *smoothness* as a measure of data conforming to the graphical model. Based on the data  $\theta[n]$ , we define the edge derivative of graph signal  $\Delta \theta[n]$  with respect to the edge  $E_{uv}$  at vertex  $u$  as

$$\left. \frac{\partial \Delta \theta[n]}{\partial E_{uv}} \right|_u \triangleq \sqrt{y_{uv}} (\Delta \theta_v[n] - \Delta \theta_u[n]). \quad (7)$$

Accordingly, the graph gradient of the graph signal  $\Delta \theta[n]$  at vertex  $u$  is defined as

$$\nabla_u \Delta \theta[n] \triangleq \left[ \frac{\partial \Delta \theta[n]}{\partial E_{uv}} \right]_u \quad (8)$$

and the *local* variation of the signal at  $u$  is defined as [21]

$$\|\nabla_u \Delta \theta[n]\|_2 \triangleq \left[ \sum_{v: E_{uv} \in E} y_{uv} (\Delta \theta_v[n] - \Delta \theta_u[n])^2 \right]^{\frac{1}{2}}. \quad (9)$$

This location variation metric provides a measure of *local smoothness* of  $\Delta \theta[n]$  around vertex  $u$ , that is a metric that quantifies the conformity of  $\Delta \theta[n]$  to the structure of the graph around vertex  $u$ . By using the local metrics, we can define a *global* smoothness of  $\Delta \theta[n]$  with respect to graph  $\mathcal{G}$  as

$$\mathcal{S}_n(\mathcal{G}) \triangleq \frac{1}{2} \sum_{u \in V} \|\nabla_u \Delta \theta[n]\|_2^2 = \Delta \theta^\top[n] \cdot \mathcal{L}_B \cdot \Delta \theta[n]. \quad (10)$$

The graph signal  $\Delta \theta[n]$  become smoother with respect to the graph  $\mathcal{G}$  if the graph signal takes closer values at neighboring vertices with non-zero weights. Hence, the conformity level of the data  $\Delta \theta[n]$  to graph  $\mathcal{G}$  increases as  $\mathcal{S}_n(\Delta \theta[n])$  decreases [22].

In the smoothness metric, the data  $\Delta\theta[n]$  is random, and  $\mathcal{L}_B$  is known. These render  $\mathcal{S}_n(\mathcal{G})$  as random variables, inheriting their randomness from  $\Delta\theta[n]$ . Considering the statistical model specified in Section II, we denote the empirical pdf of the global smoothness metric  $\mathcal{S}_n(\mathcal{G})$  by  $f$ . Furthermore, when line  $E_{uv}$  is in outage, the smoothness of observation vector with respect to the altered graph  $\mathcal{G}_{uv}$  is given by  $\mathcal{S}_n(\mathcal{G}_{uv}) = \Delta\theta^\top[n] \cdot \mathcal{L}_{B_{uv}}^\top \cdot \Delta\theta[n]$ . We denote the pdfs of  $\mathcal{S}_n(\mathcal{G}_{uv})$  by  $f_{uv}$ .

#### IV. GG-QCD: DETECTION VIA GLOBAL SMOOTHNESS

At an unknown time instant  $\gamma$  an outage occurs in an unknown transmission line  $E_{uv} \in E$ . We assume that this outage does not cause an island in the system. Hence, the post-change graph representing the system remains a connected graph. Our objective is to use the smoothness metrics  $\mathcal{S}_n(\mathcal{G})$  and design an online algorithm that forms two intertwined decisions. The first decision pertains to *detecting* whether an outage has occurred. This is essentially a binary decision. The second decision involves *localizing* the line in outage, that is, identifying the line  $E_{uv}$ . We focus on the detection decision in this section and will discuss localization in Section V. The objective of quickest detection is to detect a change with minimal delay after the outage instance  $\gamma$ . Minimizing such a delay, on the other hand, has an inherent tension with the quality of the decisions: declaring a change-point too quickly is susceptible to raising frequent false alarms, that is, declaring an outage while there is no outage in the system. Hence, designing a detection rule involves resolving a tension between the agility and quality of the decisions.

To formalize this, we have a *composite* post-change model, according to which the post-change distribution belongs to  $\{f_{uv} : (u, v) \in E\}$ . When an outage occurs, we denote  $\epsilon_{uv}$  as the prior probability that the line in outage is  $E_{uv}$ . Accordingly, we define the mixture distribution

$$g(\mathcal{S}_n(\mathcal{G})) \triangleq \sum_{(u, v) \in E} \epsilon_{uv} \cdot f_{uv}(\mathcal{S}_n(\mathcal{G})). \quad (11)$$

We define  $\tau_D \in \mathbb{N}$  as the time that we can form a confident detection decision. A canonical model to quantify the decision delay is the conditional average detection delays (CADDs) due to Pollak [23]

$$\text{CADD}(\tau_D) \triangleq \sup_{\gamma \geq 1} \mathbb{E}_\gamma [\tau_D - \gamma \mid \tau_D \geq \gamma] \quad (12)$$

where  $\mathbb{E}_\gamma$  is the expectation with respect to the probability distribution when the change happens at time  $\gamma \in (n-1, n]$ . When there is no prior assumption about when a change-point occurs, a reasonable measure of false alarms is the mean-time to false alarm, or it's reciprocal, which is the false alarm rate (FAR) defined as

$$\text{FAR}(\tau_D) \triangleq \frac{1}{\mathbb{E}_\infty[\tau_D]} \quad (13)$$

where  $\mathbb{E}_\infty$  is the expectation with respect to the distribution when a change never occurs, i.e.,  $\gamma \triangleq \infty$ . For the detection task, a standard approach to balance the trade-off between decision

delay and false alarm rates are solving [23]

$$\min_{\tau_D} \text{CADD}(\tau_D) \quad \text{subject to} \quad \text{FAR}(\tau_D) \leq \alpha \quad (14)$$

where  $\alpha \in \mathbb{R}_+$  controls the rate of false alarms. Once a detection decision is formed, we also need to localize the line in outage. For the quickest change-point detection problem with a composite post-change model, a variant of the popular cumulative sum (CuSum) algorithm enjoys optimality properties. The variant, weighted cumulative sum (W-CuSum) involves calculating

$$W_d[n] \triangleq \max_{1 \leq k \leq n+1} \sum_{i=k}^n \log \left( \frac{g(\mathcal{S}_i(\mathcal{G}))}{f(\mathcal{S}_i(\mathcal{G}))} \right) \quad (15)$$

computing which follows a convenient recursion given by

$$W_d[n] \triangleq \left( W_d[n-1] + \log \left( \frac{g(\mathcal{S}_n(\mathcal{G}))}{f(\mathcal{S}_n(\mathcal{G}))} \right) \right)^+ \quad (16)$$

where we set  $W_d[0] = 0$ . In this approach, the weighted cumulative sum sequential statistic declares a line outage at a stopping time

$$\tau_D \triangleq \inf \{n \geq 1 : W_d[n] > C_d\}. \quad (17)$$

In order to satisfy the constraint on  $\text{FAR}(\tau_D)$  in (14), we compute the threshold  $C_d$  in (17) accordingly. In particular, we run a Monte Carlo over multiple AC power flows under pre-outage conditions for a range of thresholds  $C_d$  that satisfy  $\frac{1}{\text{FAR}(\tau_D)} \triangleq \mathbb{E}_\infty(\tau_D) \approx \alpha^{-1}$ , where  $\alpha$  is given by the operator, and compute (16) for each realization until the stopping condition (17) is satisfied.

#### V. GG-QCD: LOCALIZATION VIA LOCAL SMOOTHNESS

Once an outage is declared at  $\tau_D$ , the next goal is to localize the outage. Motivated by minimizing the delay and the complexity of the localization routine, we devise a framework with two key ideas:

**1) Retrospective Change Detection:** Note that the detection stopping time  $\tau_D$  is the instance at which we had sufficient confidence that an outage has occurred prior to  $\tau_D$ . This indicates that if we can estimate the actual change-point  $\gamma$ , then all the samples at  $n \in \{\gamma, \dots, \tau_D\}$  are drawn from the post-change model. To avoid further delay imposed by collecting fresh samples, we can first re-use all the samples  $\{\Delta\theta[n] : n \in \{\gamma, \dots, \tau_D\}\}$ , and only take fresh samples if these are inconclusive for localization. To this end, a pivotal objective is estimating  $\gamma$ , i.e., retrospect detection of the change-point.

**2) Active Graph Clustering:** A direct approach to localization would be testing the lines individually, rendering  $L$  parallel tests. In contrast, we perform active graph clustering to estimate a small proximity in which the outage is deemed to lie. This is then followed by testing only the lines contained in the estimated outage proximity. This reduces the number of tests from  $L$  to about  $\log_2(L)$ . Next, we discuss each of these two steps and the final localization rules.

### A. Retrospective Change-Point Detection (RCPD)

We start by performing retrospective change-point detection (RCPD) to estimate  $\gamma$  based on the available data when it is deemed a change has occurred. The existing approaches to RCPD include a non-parametric approach in [24], Bayesian approach in [25], [26], and a quasi-Bayesian formulation in [27]. Our objective involves forming two intertwined decisions. We aim to estimate the change-point. This decision predicates on ensuring that a change has, in fact, occurred. Hence, we face the combined decision of detecting a change and then estimating the change-point. By defining  $\mathcal{S}_{1:\tau_D} \triangleq \{\mathcal{S}_d(\mathcal{G}) : d \in \{1, \dots, \tau_D\}\}$ , the combined decision is a solution to the following composite hypothesis testing problem:

$$\begin{aligned} \mathcal{H}_0 : \mathcal{S}_{1:\tau_D} &\sim \prod_{n=1}^{\tau_D} f(\mathcal{S}_n(\mathcal{G})) \\ \mathcal{H}_1 : \mathcal{S}_{1:\tau_D} &\sim \prod_{n=1}^{\gamma-1} f(\mathcal{S}_n(\mathcal{G})) \cdot \prod_{n=\gamma}^{\tau_D} g(\mathcal{S}_n(\mathcal{G})) \end{aligned} \quad (18)$$

where  $\mathcal{H}_0$  accounts for no change-point by  $\tau_D$ , and  $\mathcal{H}_1$  indicates otherwise. When decided in favor of  $\mathcal{H}_1$ , we also estimate  $\gamma$ . As established in [26], the rule for discerning  $\mathcal{H}_0$  and  $\mathcal{H}_1$  is

$$\max_{\zeta \in \{1, \dots, \tau_D\}} \pi_\zeta \prod_{n=\zeta}^{\tau_D} \frac{g(\mathcal{S}_n(\mathcal{G}))}{f(\mathcal{S}_n(\mathcal{G}))} \stackrel{\mathcal{H}_0}{\leqslant} \lambda \quad (19)$$

where  $\pi_\zeta \triangleq \mathbb{P}(\zeta \mid \tau_D = d)$  is the prior probability of  $\zeta$  being the change-point. Furthermore, the maximum a-posteriori (MAP) estimate of  $\gamma$  is given by

$$\hat{\gamma}_{\text{MAP}} = \arg \max_{\zeta \in \{1, \dots, \tau_D\}} \pi_\zeta \prod_{n=\zeta}^{\tau_D} \frac{g(\mathcal{S}_n(\mathcal{G}))}{f(\mathcal{S}_n(\mathcal{G}))}. \quad (20)$$

To analyze the prior  $\pi_\zeta$ , we note that (17) is satisfied prior to the start of the localization process. In particular, since we have high confidence that a change has occurred, it is highly likely to be within a short interval preceding  $\tau_D$ . Hence, we assume the prior to be binomially distributed with parameter  $p$ , where  $p$  can be obtained from historical data. For instance, by fitting the expected values,  $p \cdot \tau_D$  (the expected value of the binomial distribution) equals the historical average of detection delay, i.e.,  $(\tau_D - \gamma)$ , yielding  $p = 1 - \frac{\gamma}{\tau_D}$ . We define  $\hat{\gamma}$  as the estimate for the change-point  $\gamma$  following.

### B. Spectral Bisection Graph Partitioning

Upon estimating  $\gamma$ , and by using the samples  $\{\Delta\theta[n] : n \in \{\hat{\gamma}, \dots, \tau_D\}\}$ , and possibly more fresh samples when deemed necessary, we aim to localize the line in outage. For this purpose, we take an active partitioning approach to iteratively eliminate the parts of the graph deemed not to contain a faulty line and progressively focus on the more promising parts. This iterative process starts by partitioning the graph  $\mathcal{G} = (V, E, \mathbf{B})$  to two subgraphs  $\mathcal{G}^r \triangleq (V^r, E^r, \mathbf{B}^r)$ , where  $r \in \{1, 2\}$  followed by a quickest detection approach to determine which partition is more likely to contain the faulty line. In the next iteration, this partition is further bisected for more scrutiny, and this process continues

until we cannot further partition the surviving subgraph into two meaningful partitions, i.e., the surviving subgraph has no more than four vertices.

To formalize the iterative bisection search process, we define  $\mathcal{G}_i$  as the subgraph survived after that  $i^{\text{th}}$  iteration, and we set  $\mathcal{G}_0 = \mathcal{G}$ . In the  $(i+1)^{\text{th}}$  iteration, we partition  $\mathcal{G}_i$  into  $\mathcal{G}_i^1$  and  $\mathcal{G}_i^2$ , and retain one of them, denoted  $\mathcal{G}_{i+1}$ , for further scrutiny in the next iteration. Based on these notations, next we discuss how to partition  $\mathcal{G}_i$ , and how to specify  $\mathcal{G}_{i+1}$ . All these decisions are data-driven, and our objective is to form the decision with the fewest number of samples.

**Partitioning  $\mathcal{G}_i$ :** We employ a spectral graph partitioning algorithm for partitioning  $\mathcal{G}_i \triangleq (V_i, E_i, \mathbf{B}_i)$ . For simplicity of notations, we assume that  $N_i \triangleq |V_i|$  is even, and the odd cases can be addressed with minor adjustments. Corresponding to the set of nodes  $V_i$ , we define the  $N_i$ -dimensional vector  $\mathbf{p}_i$  as the partitioning vector if  $\mathbf{p}_i \in \mathcal{P}_i \triangleq \mathcal{C}_i \cap \mathcal{B}_i$ , where we have defined

$$\mathcal{C}_i \triangleq \{\mathbf{p}_i \in \{\pm 1\}^{N_i}\}, \text{ and}$$

$$\mathcal{B}_i \triangleq \left\{ \mathbf{p}_i \in \mathbb{R}^{N_i} : \sum_{j=1}^{N_i} \mathbf{b}_i[j] = 0 \right\}.$$

The condition  $\mathbf{p}_i \in \mathcal{C}_i$  designates a binary partition of graph  $\mathcal{G}_i$  such that when  $\mathbf{p}_i[j] = -1$ , the  $j^{\text{th}}$  element of  $V_i$  will be placed in partition  $\mathcal{G}_i^1$ , and otherwise, when  $\mathbf{p}_i[j] = 1$ , it will be placed in  $\mathcal{G}_i^2$ . On the other hand, the condition  $\mathbf{p}_i \in \mathcal{B}_i$  ensures that the partitions are balanced with an equal number of nodes. Our objective is to find a partition vector  $\mathbf{p}_i \in \mathcal{P}_i$  in order to partition  $\mathcal{G}_i$ . An optimal choice of  $\mathbf{p}_i$  that ensures maximal independence between the two partitioned subgraphs can be found as the solution to

$$\mathbf{p}_i^* \triangleq \arg \min_{\mathbf{p}_i \in \mathcal{P}_i} \sum_{(u,v) \in E_i} y_{uv} \cdot (\mathbf{p}_i[u] - \mathbf{p}_i[v])^2 \quad (21)$$

$$\triangleq \arg \min_{\mathbf{p}_i \in \mathcal{P}_i} \mathbf{p}_i^\top \cdot \mathcal{L}_{\mathbf{B}_i} \cdot \mathbf{p}_i. \quad (22)$$

As shown in [28] and [29], solving (22) is NP-hard. An approximate solution to (22) can be obtained by relaxing the discreteness constraint on the set  $\mathcal{C}_i$  rendering the modified problem:

$$\tilde{\mathbf{p}}_i^* \triangleq \arg \min_{\mathbf{p}_i \in \mathcal{B}_i, \|\mathbf{p}_i\|_2^2 \triangleq 1} \mathbf{p}_i^\top \cdot \mathcal{L}_{\mathbf{B}_i} \cdot \mathbf{p}_i. \quad (23)$$

An effective solution to  $\tilde{\mathbf{p}}_i^*$  is obtained by considering  $\tilde{\mathbf{p}}_i^* \triangleq \mathbf{e}_i$  where  $\mathbf{e}_i$  denotes the Fiedler vector (i.e., the eigenvector associated with the second smallest eigenvalue) of the Laplacian matrix  $\mathcal{L}_{\mathbf{B}_i}$ . This is because the eigenvector associated with the smallest eigenvalue of the Laplacian matrix is a constant vector, which if used, will not yield any partitions for graph  $\mathcal{G}_i$ . As established in [29], an approximate solution to  $\tilde{\mathbf{p}}_i^*$  is obtained by setting all the elements of  $\tilde{\mathbf{p}}_i^*$  above the median of  $\mathbf{e}_i$ , denoted by  $\bar{\mathbf{e}}_i$ , to  $(+1)$  and all the elements of  $\tilde{\mathbf{p}}_i^*$  below  $\bar{\mathbf{e}}_i$  to  $(-1)$ , resulting in an approximation for  $\tilde{\mathbf{p}}_i^*$  that belongs to  $\mathcal{P}_i$ . By constructing the median-cut vector  $\mathbf{p}_i^*$ , two evenly partitioned subgraphs are obtained by mapping each entry in  $\mathbf{p}_i^*$  of opposite signs to two distinct graph partitions. We note that in order to obtain viable Laplacian matrices  $\mathcal{L}_{\mathbf{B}_i^1}$  and  $\mathcal{L}_{\mathbf{B}_i^2}$  we discard all

**Algorithm 1:** Bisecting Graph  $\mathcal{G}_i$  to  $\mathcal{G}_i^1$  and  $\mathcal{G}_i^2$ .

---

```

1: Input graph  $\mathcal{G}_i$ 
2: Initialize  $V_i^1 \leftarrow \emptyset$ ,  $V_i^2 \leftarrow \emptyset$ 
3: Construct Laplacian matrix  $\mathcal{L}_{\mathbf{B}_i}$  of weight matrix  $\mathbf{B}_i$ 
4: Compute the Fiedler vector  $\mathbf{e}_i$  of  $\mathcal{L}_{\mathbf{B}_i}$ 
5: for every node  $k$  in  $V$  do
6:   if  $\mathbf{e}_i[k] \leq \bar{\mathbf{e}}_i$  then
7:      $V_i^1 \leftarrow V_i^1 \cup \{k\}$ 
8:   else
9:      $V_i^2 \leftarrow V_i^2 \cup \{k\}$ 
10:  end if
11: end for
12: if  $||V_i^1| - |V_i^2|| > 1$  then
13:   Adjust for nodes in set  $V_i^1$ ,  $V_i^2$  to make the
      difference atmost 1
14: end if
15: Construct  $E_i^r$ 
16: return  $\mathcal{G}_i^1$  and  $\mathcal{G}_i^2$ 

```

---

the inter-connected edges (tie-lines) between  $\mathcal{G}_i^1$  and  $\mathcal{G}_i^2$  in the current iteration, and devise independent localization decision rules for tie-lines in Section V-C. Note that the assumption of  $N_i$  being even is made only for convenience and that a graph can be partitioned into two approximately equal sets following Algorithm 1.

**Filtration:** Given partitions  $\mathcal{G}_i^1$  and  $\mathcal{G}_i^2$ , next we decide to discard one and retain the other for further scrutiny. We develop a quickest change detection approach and apply it to subgraphs  $\mathcal{G}_i^1$  and  $\mathcal{G}_i^2$ . To formalize this, upon finding  $\mathcal{G}_i^1$  and  $\mathcal{G}_i^2$ , we define  $\mathcal{S}_n(\mathcal{G}_i^r)$  as the local smoothness metric as follows:

$$\mathcal{S}_n(\mathcal{G}_i^r) = \Delta \boldsymbol{\theta}_i^{r\top} [n] \cdot \mathcal{L}_{\mathbf{B}_i^r} \cdot \Delta \boldsymbol{\theta}_i^r [n] \quad \text{for } r \in \{1, 2\} \quad (24)$$

where  $\boldsymbol{\theta}_i^r[n]$  denotes the vector of phase angle measurements associated with the buses in subgraph  $\mathcal{G}_i^r$ . We denote the pre-change empirical pdf of the local smoothness  $\mathcal{S}_n(\mathcal{G}_i^r)$  by  $f_i^r$  and denote the post-outage empirical pdf of  $\mathcal{S}_n(\mathcal{G}_i^r)$  when line  $E_{uv} \in E_i^r$  is in outage by  $g_{i,uv}^r$ . When an outage occurs, we denote the prior probability of line  $E_{uv} \in E_i^r$  being in outage by  $\epsilon_i^r[u, v]$ , and accordingly, define the post-change mixture distribution as

$$g(\mathcal{S}_n(\mathcal{G}_i^r)) = \sum_{(u,v) \in E_i^r} \epsilon_i^r[u, v] \cdot g_{i,uv}^r(\mathcal{S}_n(\mathcal{G}_i^r)). \quad (25)$$

Corresponding to each of the two subgraphs, we define the following W-CuSum statistic  $\forall r \in \{1, 2\}$  and  $\forall n \geq \hat{\gamma}$ :

$$W_i^r[n] \triangleq \left( W_i^r[n-1] + \log \left( \frac{g(\mathcal{S}_n(\mathcal{G}_i^r))}{f_i^r(\mathcal{S}_n(\mathcal{G}_i^r))} \right) \right)^+ \quad (26)$$

where the statistics  $W_i^r[\hat{\gamma} - 1] = 0 \forall r \in \{1, 2\}$ . The W-CuSum statistic declares an outage in subgraph  $\mathcal{G}_i^r$  at time instant  $\tau_i^r$  defined

$$\tau_i^r \triangleq \inf\{n \geq \hat{\gamma} : W_i^r[n] > C_i^r\} \quad (27)$$

where constant  $C_i^r$  controls the rate of false alarm events. The test statistics associated with each of the two-subgraphs are run in parallel, and the subgraph that first identifies an outage is

**Algorithm 2:** Bisection Search.

---

```

1: Input  $\mathcal{G}$ , set  $i \triangleq 1$ ,  $\mathcal{G}_0 \triangleq \mathcal{G}$ 
2: Run Algorithm-1 on  $\mathcal{G}_{i-1} \rightarrow \mathcal{G}_{i-1}^1, \mathcal{G}_{i-1}^2$ 
3: Find  $\tau_{i-1} \triangleq \min\{\tau_{i-1}^1, \tau_{i-1}^2\}$  using (27)
4: Find  $r^* \triangleq \arg \min \tau_{i-1}^r$ 
5: Set  $\mathcal{G}_i = \mathcal{G}_{i-1}^{r^*}$ 
6: if  $|\mathcal{V}_i| > 4$  then
7:   Set  $i \leftarrow i + 1$  & go to 2:
8: end if
9: Output  $\mathcal{G}_i$ 

```

---

selected for more scrutiny, and the other subgraph is discarded permanently. The details of the active bisection search are provided in Algorithm-2.

*C. Terminal Decision Rule for Line Outage Localization*

While the bisection search algorithm discussed in Section V-B provides the most likely subgraph in which the outage is deemed to lie, it does not provide the terminal decision rule  $\delta$ . Moreover, it does not incorporate the possibility of an outage in tie-lines that were discarded to form viable Laplacian matrices. To address these issues, we employ parallel CuSum tests customized to each line in the resulting subgraph obtained at the end of Algorithm-2 and each tie-line obtained in the  $i^{\text{th}}$  iteration of Algorithm-2. We note that since the number of lines in the subgraph obtained at the end of Algorithm-2 is guaranteed to be small in number, running parallel tests renders minimal complexity. Similarly, since the number of lines between two subgraphs in any iteration of Algorithm-2 is significantly fewer in number compared to the internal lines in the two respective subgraphs, running parallel tests for tie-lines contributes minimally to the complexity. We denote the set  $E_{T_i}$  by the set of tie-lines obtained in the  $i^{\text{th}}$  iteration.

We define a CuSum statistic formed by a simple pre- and post-change global smoothness models  $\mathcal{S}_n(\mathcal{G}) \sim f$ , and  $\mathcal{S}_n(\mathcal{G}) \sim f_{uv}$  respectively, when line  $E_{uv} \in E$  is in outage and define

$$W_i^{uv}[n] \triangleq \left( W_i^{uv}[n-1] + \log \left( \frac{f_{uv}(\mathcal{S}_n(\mathcal{G}))}{f(\mathcal{S}_n(\mathcal{G}))} \right) \right)^+ \quad \forall n \geq \hat{\gamma}. \quad (28)$$

where  $W_i^{uv}[\hat{\gamma} - 1] = 0$ . We declare an outage for  $E_{uv}$  at the stopping time  $\tau_i^{uv}$  defined as

$$\tau_i^{uv} \triangleq \inf\{n \geq \hat{\gamma} : W_i^{uv}[n] > C_i^{uv}\}. \quad (29)$$

where  $C_i^{uv}$  controls the false alarm rate. We augment Algorithm 2 by running the tests associated with all the tie-lines in (28) and the two subgraphs in (26) in parallel in the  $i^{\text{th}}$  iteration of Algorithm-2 and subsequently declare an outage at time instant  $\tau_i$  given by

$$\tau_i \triangleq \min\{\tau_i^r, \tau_i^{uv} : \forall r \in \{1, 2\}, \forall E_{uv} \in E_{T_i}\}. \quad (30)$$

Following the stopping rule (30), if a tie-line is declared to be in outage, i.e.,  $\tau_i = \tau_i^{uv}$ , prior to the stopping condition of

**Algorithm 3:** Algorithm for Line Outage Localization.

```

1:  $i \leftarrow 0$ 
2: while  $W_d > C_d$  do
3:   Estimate  $\hat{\gamma}$ 
4:   procedure Binary _ Search ( $\mathcal{G}$ )
5:      $i \leftarrow i + 1$ 
6:     if  $|V_i| \leq 4$  then
7:       for all  $\forall E_{uv} \in E_i$  do in parallel,
8:       Compute  $W_i^{uv}[n]$  from (28)
9:     end for
10:    Compute  $\tau_{i_{\max}}$  from (31)
11:     $\delta(\tau_L) \leftarrow E_{uv}$ 
12:    break;
13:  else
14:    Bisect  $\mathcal{G}_i$  to obtain  $\mathcal{G}_i^1, \mathcal{G}_i^2$  and tie-lines using
        Algorithm-1
15:    Run statistics (26), (28) in parallel
16:    Compute  $\tau_i$  from (30)
17:    if  $\tau_i \triangleq \tau_i^r$  then
18:      procedure Binary _ Search( $\mathcal{G}_i^r$ )
19:    else
20:       $\tau_L = \max(\tau_D, \tau_0, \dots, \tau_i)$ 
21:       $\delta(\tau_L) \leftarrow E_{uv}$ 
22:    end if
23:  end if
24: end procedure
25: return  $\delta$ 
26: end while

```

Algorithm-2, the terminal decision rule about the line hypothesized in outage is given by  $\delta(\tau_L) \triangleq E_{uv}$  and the data acquisition process is terminated at time instant  $\tau_L = \max(\tau_D, \tau_0, \dots, \tau_i)$ . If  $\tau_i = \tau_i^r$ , then the subgraph  $\mathcal{G}_i$  (Step 5, Algorithm-2) is bisected recursively. If, however, the stopping condition  $|V_i| \leq 4$  is realized, statistics (28) associated with all the tie-lines in subgraph  $\mathcal{G}_i$  are run in parallel for which the stopping rule is given by

$$\tau_{i_{\max}} \triangleq \min\{\tau_i^{uv} : \forall E_{uv} \in E_i\}. \quad (31)$$

Algorithm-3 summarizes the line outage localization algorithm.

**VI. CASE STUDIES AND DISCUSSION**

We illustrate the performance of the proposed line outage detection and identification algorithm on IEEE benchmark test cases. Specifically, we consider the 30- and 118-bus power system test cases and employ the simulation tool MATPOWER [30] throughout to solve for the voltage phase angles by repeatedly solving AC power flows at each time instant  $n$ . We note that a consequence of using MATPOWER is that a line outage causes a step change in phase angles that is in contrast to realistic scenarios where PMUs consist of anti-aliasing filters that only allow for gradual changes in measurements. In this regard, we acknowledge a requirement for pre-processing real-time measurements in order to apply Algorithm-3 to realistic phasor data, a topic of future work. To simulate the detection and

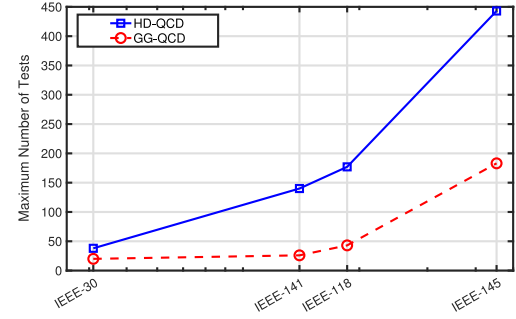


Fig. 1. Maximum number of statistical tests required against the number of transmission lines in standard IEEE test cases.

localization delays, we assume a change point  $\gamma \triangleq 100$ . Note that we consider only line outages that do not induce islands in the anomalous network. We assume that the power-injections satisfy  $(\mathbf{P} + \Delta\mathbf{P})[n] \sim \mathcal{N}(\mathbf{P}, \sigma_0^{-2}\mathbf{I})$ , where  $\mathbf{P}$  is the nominal power-injection vector, however, we note that this is not a strict assumption and that our framework can incorporate other correlation structures and other arbitrary pdfs for  $\Delta\mathbf{P}$  as we learn the empirical densities of the smoothness metrics from data. We note that the decision rules for outage detection and localization depend on the empirical statistical densities of the global and local smoothness metrics, which we estimate from historical data. In this paper, we assume  $\sigma_0^{-2} = 0.5$  for the IEEE-30 bus,  $\sigma_0^{-2} = 0.002$  for the IEEE-118 bus and assume a sampling rate of 120 samples per second.

**A. Computational Complexity and Scalability**

We start by assessing the computational complexity and the scalability of the GG-QCD algorithm. While testing lines individually in [14] is expected to have an overall lower average detection delay, the complexity of that becomes quickly prohibitive as the system's size grows. Specifically, running individual tests requires running  $L$  parallel tests at all times; while our approach runs only one test when there is no outage and about  $\log_2(L)$  tests when there is an outage. First, we compare the *maximum* number of tests required for precisely localizing an outage event. Figure 1 compares the maximum number of tests required versus the number of transmission lines in the standard IEEE test cases. We note that since in our approach, the number of statistical tests required is a function of the geographical location of the line in the network, we plot the number of tests required in the worst case. From Fig. 1, it is evident that employing the proposed approach requires a fewer number of tests. We note that, on average, the number of tests required would be significantly fewer than that of the worst case that is plotted in Fig. 1.

Furthermore, we show that each of the individual tests in our approach is also less computationally complex. To quantify the computational complexity of our proposed algorithm, we compare the complexities of individual tests and provide running times for the respective algorithms. Specifically, we compare the complexities of the individual tests required for multiple IEEE test cases. Since line outages are rare events, we compare the algorithms' run-times by running the respective test statistics

TABLE I  
RUN-TIMES (RTs) IN SECONDS OF ALGORITHMS UNDER PRE-OUTAGE NETWORK CONDITIONS  $n = 10000$  ITERATIONS FOR VARIOUS TEST CASES

IEEE test case	Run-time (GG-QCD)	Run-time (HD-QCD)
3-bus	0.11	0.29
5-bus	0.23	1.01
6-bus	0.44	2.23
30-bus	1.52	—
118-bus	7.61	—

under pre-change network conditions, i.e., when there is no outage in the network for  $n = 10000$  iterations. At each time instant  $n$ , we compute the time it takes to update the CuSum statistics associated with each of the algorithms. We note that when comparing the computational time with other HD-QCD approaches, we generate a new observation at every time instant  $n$  from the histograms of the learnt models for both HD-QCD and GG-QCD methods, to have a fair comparison. The histograms of the models are generated such that the number of bins, in every dimension of the histogram, in both methods are the same. Table I summarizes the run-times.

It is observed that even for a small-size model, the discrepancy in computational time is significant. Such a discrepancy grows significantly as the size of the network increases due to the following two underlying reasons: (i) while both the methods compute likelihood ratios associated with each transmission line as part of their CuSum statistic, HD-QCD methods query the histograms in each dimension in order to compute the joint distribution of  $\Delta\theta$ , and (ii) the global and local smoothness summary statistic in the GG-QCD approach is always one-dimensional irrespective of the size of the network. We note that the computational time for 30 and 118-bus models are not reported since their respective 29 and 117 dimensional histograms impose memory restrictions.

### B. Detection and Localization Delays

Next, we assess the efficiency of detecting and localizing outages and compare the performance against those of HD-QCD approaches. The key observation is that the cost of a significant improvement in computational complexity is a graceful degradation in the detection and localization delays. We note that the localization delay is the delay associated with uniquely localizing the line in outage, i.e., it incorporates the detection delay. To capture the overall performance, we consider two kinds of line outages: (i) line outages that belong to different geographical locations (internal and tie-lines), and (ii) line that render highest, lowest and intermediate localization delays.

First, we consider outage events based of the geographical location. Accordingly, we consider outage events for lines  $E_{4,12}$ ,  $E_{18,19}$ ,  $E_{10,17}$  in the 30-bus and outage events in lines  $E_{38,65}$ ,  $E_{65,68}$ , and  $E_{24,70}$  in the 118-bus system. We note that, in the 30- and 118-bus system, there are a total of 41 and 186 lines, respectively, out of which there exist 3 and 9 lines that cause islands in the network. Therefore, we weight the prior

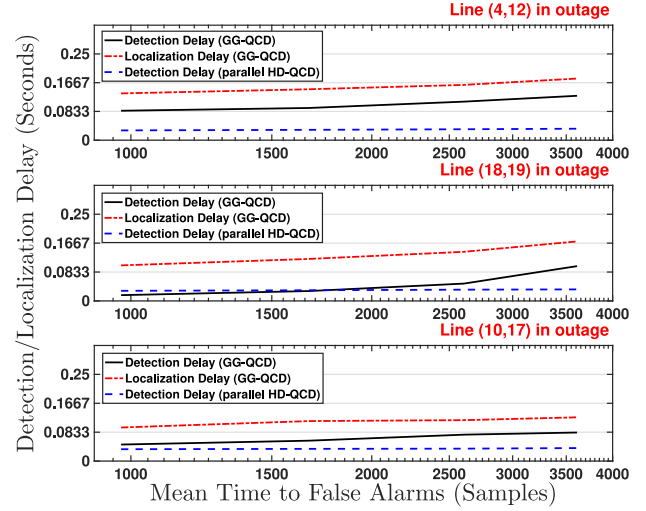


Fig. 2. Comparison of average delays versus MTFA (30-bus).

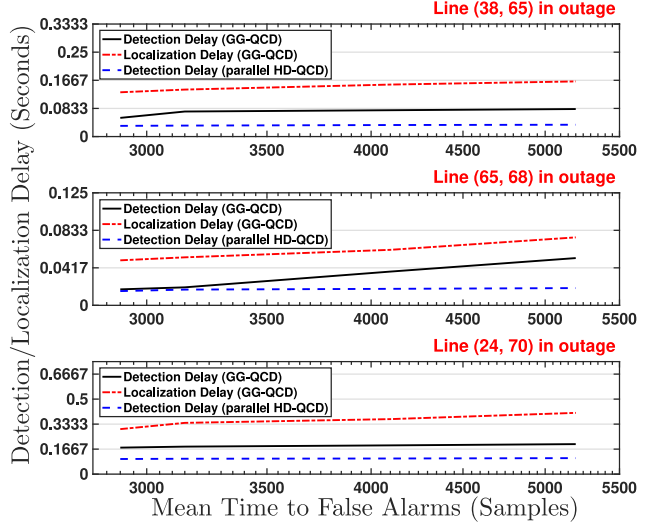


Fig. 3. Comparison of average delays versus MTFA (118-bus).

on each outage hypothesis by  $\epsilon_{uv} \triangleq \frac{1}{38}$  and  $\epsilon_{uv} \triangleq \frac{1}{177}$  for 30- and 118-bus systems, respectively, when computing test statistics (16). Thresholds  $C_d$  specified in (17) are chosen such that the mean-time to false alarm (MTFA) value lie in the range [900, 3600] and [2900, 5200] in samples for the 30- and 118-bus systems, respectively. Accordingly, thresholds  $C_i^r$  associated with all the subgraphs  $\mathcal{G}_i^r$  and thresholds  $C_i^{uv}$  associated with all the tie-lines are computed. We run a Monte-Carlo simulation on 5000 random paths to compute the average detection and localization delay for each considered line in outage corresponding to the chosen thresholds. Figures 2 and 3 show the performance curves that essentially captures the trade-off between false alarm rate and average delay. We observe that increasing the thresholds increases the mean-time to false alarms while penalizes the average detection and localization delay. We also observe a detection-localization delay gap owing to the design of the decision rules  $\delta$  discussed in Section V-C.

TABLE II  
OVERALL LOCALIZATION DELAYS (IN SECONDS) CAPTURED VIA EMPIRICAL ALD THROUGH NUMERICAL EVALUATIONS (30-BUS)

MTF (Samples)	1,000	1,600	2,600	3,600
Line (6,9) outage	0.076	0.078	0.081	0.082
Line (6,8) outage	0.143	0.149	0.161	0.185
Line (3,4) outage	0.310	0.321	0.328	0.335

TABLE III  
OVERALL LOCALIZATION DELAYS (IN SECONDS) CAPTURED VIA EMPIRICAL ALD THROUGH NUMERICAL EVALUATIONS (118-BUS)

MTF (Samples)	1,000	1,600	2,600	3,600
Line (24,72) outage	0.042	0.043	0.044	0.046
Line (55,56) outage	0.451	0.462	0.467	0.476
Line (34,37) outage	2.512	2.561	2.578	2.593

In particular, we observe that internal line outages that render very low detection delays lead to relatively higher localization delays. This is because for such lines, there exist very few to no past samples to re-use and therefore, further iterations of active clustering result in the collection of fresh samples that penalizes the localization delay every iteration. Internal lines (18,19) and (3,4) in the 30-bus system are examples that render a relatively large detection-localization gap despite having minimal detection delays. Localization delays for the 30-bus are also tabulated in Table IV for further studies and comparison.

Figure 7 visually illustrates how the 30-bus system is successively bisected, resulting in a 4-node graph after three iterations when line  $E_{10,17}$  undergoes an outage. The true line in outage is identified by running (28) for lines  $E_{10,17}$ ,  $E_{10,20}$  and  $E_{19,20}$  in parallel and evaluating the decision rule that satisfies (31).

Second, we consider outage events based on the overall localization delay that consists of the highest, lowest and intermediate average localization delays (ALDs) for lines in the 30- and 118-bus system. In case of the 30-bus system, as tabulated in Table II, we observe that outage of lines (6,9) and (3,4) lead to the lowest and highest localization delays, respectively, and that the outage of line (6,8) was chosen to be representative for intermediate delay values. Similarly, Table III tabulates the overall performance of the 118-bus system. Overall, we observe that Algorithm-3 provides reasonable localization delays, as desired.

Next, we compare the average localization delay of our algorithm to that of a HD-QCD algorithm studied in [14]. In figures 2 and 3 we observe that the HD-QCD algorithm consistently provides lower delays. Nevertheless, the delay gaps are rather marginal. For instance, in the transmission line (4,12) in the 30-bus system, the delay gap varies in the range [10,15] samples which with the assumed sampling rate, translates to less than 0.12 seconds of delay. For other lines, this difference is smaller. We remark that this is the cost for achieving a significantly lower computational complexity as addressed in Section VI-A.

TABLE IV  
PERFORMANCE OF ALGORITHM-3 UNDER NOMINAL POWER SYSTEM CONDITION (30-BUS)

MTF (Samples)	1,000	1,600	2,600	3,600
Line (4,12) outage				
LEP	0.014	0.008	0.004	0.002
ALD (sec)	0.135	0.147	0.160	0.178
Line (18,19) outage				
LEP	0.020	0.007	0.004	0.002
ALD (sec)	0.095	0.121	0.141	0.171
Line (10,17) outage				
LEP	0.008	0.006	0.004	0.002
ALD (sec)	0.096	0.109	0.118	0.126
Line (3,4) outage				
LEP	0.021	0.015	0.009	0.003
ALD (sec)	0.310	0.321	0.328	0.335

### C. Accuracy of Outage Localization

Next, we discuss the efficiency (accuracy) of the localization Algorithm-3. To quantify the quality of the terminal decision  $\delta(\tau_L)$ , we define localization error probability (LEP) as

$$\text{LEP}(\tau_L) \triangleq \mathbb{P}(\delta \neq E_{uv} | \text{outage in } E_{uv}) = \mathbb{P}_{uv}(\delta \neq E_{uv}) \quad (32)$$

where  $\mathbb{P}_{uv}$  is the probability measure of the data when line  $E_{uv}$  is in outage. To assess the variation of  $\text{LEP}(\tau_L)$  with the average localization delay, we appropriately choose thresholds as discussed in Section VI-B and numerically evaluate the LEPs over for a wide range of thresholds, thus varying the average delay, by running a Monte-Carlo simulation on 5000 random paths. Table IV and Fig. 6 plot the trade-off for different line outages in the 30- and 118-bus system, respectively. It is observed that the ALD decreases at the expense of increasing the LEP. As observed from the plots, the LEPs are within acceptable limits despite the relatively small range for MTFA.

### D. Effect of Sudden Load and Generation Change

The line outage localization algorithm (Algorithm-3) relies on the change in pdf of the observations  $\Delta\theta$ . The pdfs depend on the real-time network topology of the grid and the statistical properties of random fluctuations in real-power across the buses. While the network topology is invariant to random load-generation fluctuations, we test whether a large load or generator outage results in enough movement of the detection statistic  $W_d$  prior to triggering the binary search for localization. As discussed in (16),  $W_d[n]$  is employed to determine the presence of a line outage if the condition in (17) is met. In this regard, we simulate other outage events to test its impact on  $W_d[n]$ . Specifically, we consider the 30-bus system and simulate the following two outage scenarios: (i) a simultaneous outage of generators at buses 2,4 and outage of loads at buses 2,7 at time instant  $\gamma \triangleq 100$ , and (ii) an outage of line (3,4) at time instant  $\gamma \triangleq 100$ , for a given MTFA. Figures 4 and 5 plot the evolution of the detection statistic  $W_d[n]$ . We observe that there exists a movement in

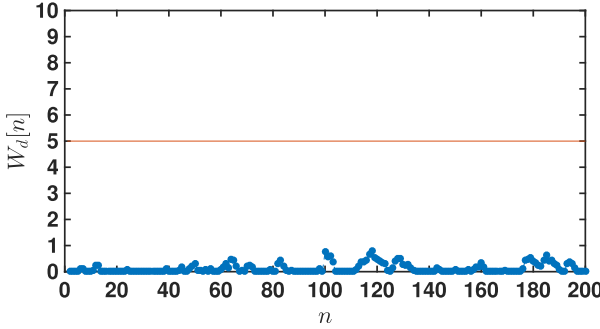


Fig. 4. A realization capturing the evolution of the detection statistic  $W_d[n]$  for a system that has undergone generator and loads outages.

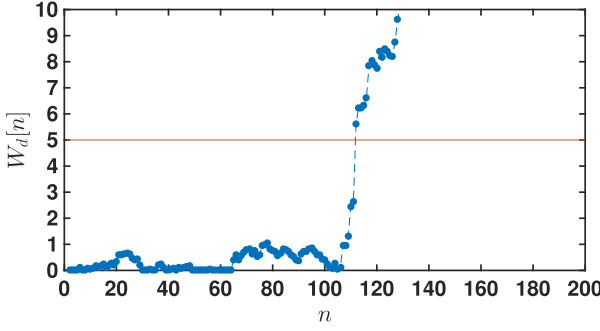


Fig. 5. A realization capturing the evolution of the detection statistic  $W_d[n]$  for a system that has undergone a line outage.

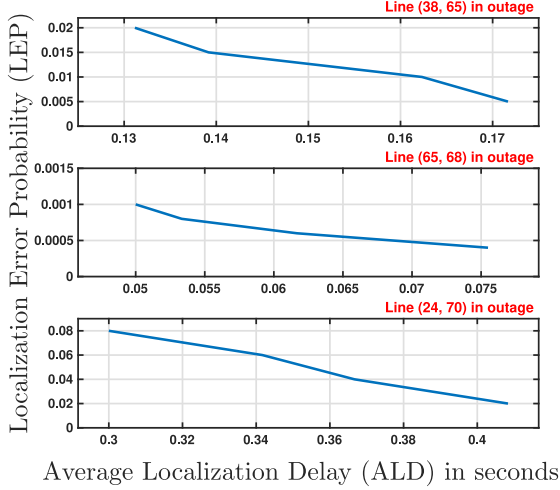


Fig. 6. LEP versus ALD (118-bus).

$W_d[n]$  at  $\gamma \triangleq 100$  in Fig 4, however,  $W_d[n]$  does not exceed the threshold  $C_d$ . In the case of a line outage,  $W_d[n]$  crosses the threshold as shown in Fig 5. We note that this is expected since changes in load and generation do not alter the pdf of the measurements  $\Delta\theta$ .

#### E. Detection and Localization Under Stressed Power System Conditions

Line outages are more likely to be caused under stressed power system conditions. Since Algorithm-3 was formulated considering the DC power flow model (Section II-A), it is imperative

TABLE V  
PERFORMANCE OF THE ALGORITHM-3 UNDER STRESSED POWER SYSTEM CONDITION (30-BUS)

MTF (Samples)	1,000	1,600	2,600	3,600
Line (4,12) outage				
LEP	0.07	0.06	0.02	0.018
ALD (sec)	0.142	0.150	0.171	0.186
Line (18,19) outage				
LEP	0.04	0.03	0.02	0.02
ALD (sec)	0.123	0.144	0.160	0.184
Line (10,17) outage				
LEP	0.03	0.02	0.012	0
ALD (sec)	0.113	0.118	0.126	0.136
Line (3,4) outage				
LEP	0.30	0.278	0.23	0.21
ALD (sec)	0.376	0.389	0.394	0.402

to analyze its performance in a highly likely scenario where the conditions are further deviated from the conventional DC power flow assumptions. While Section VI-B and VI-C show the performance under nominal power systems conditions, we consider the evaluation of Algorithm-3 under stressed conditions. In particular, we test the performance of our algorithm where we scale the loads in the system such that all load buses operate at the lowest acceptable voltage of 0.95 per unit and consider the 30-bus system. Table IV tabulates the performance metrics for the 30-bus system under nominal power system conditions that serves as a benchmark for comparison and Table V tabulates the performance metrics under stressed power systems conditions. We observe that there is a negligible difference in ALD while an increase in the LEPs. However, the error probabilities despite the stressed conditions are small, as desired.

#### F. Double Line Outage Detection and Localization for Line Outages in Close Neighborhood

We further extend the GG-QCD framework to *detect* an arbitrary double line outage while *localizing* double line outages that occur in a close neighborhood without incurring combinatorial complexity for outage localization. Consider the outage of lines  $E_{uv}, E_{ab} \in E$ . The equivalent mixture distribution for outage detection, similar to that of (11), given by

$$g(\mathcal{S}_n(\mathcal{G})) \triangleq \sum_{(u,v),(a,b) \in E} \epsilon_{uv,ab} \cdot f_{uv,ab}(\mathcal{S}_n(\mathcal{G})) \quad (33)$$

captures all possible double line outages where the post-change pdf belongs to  $\{f_{uv,ab} : (u,v), (a,b) \in E\}$ , making it viable to detect such outages. We note that in order to localize an arbitrary double line outage, it is always possible to run  $\binom{L}{2}$  test statistics  $W^{uv,ab}[n]$ , given by

$$W^{uv,ab}[n] \triangleq \left( W^{uv,ab}[n-1] + \log \left( \frac{f_{uv,ab}(\mathcal{S}_n(\mathcal{G}))}{f(\mathcal{S}_n(\mathcal{G}))} \right) \right)^+ \quad (34)$$

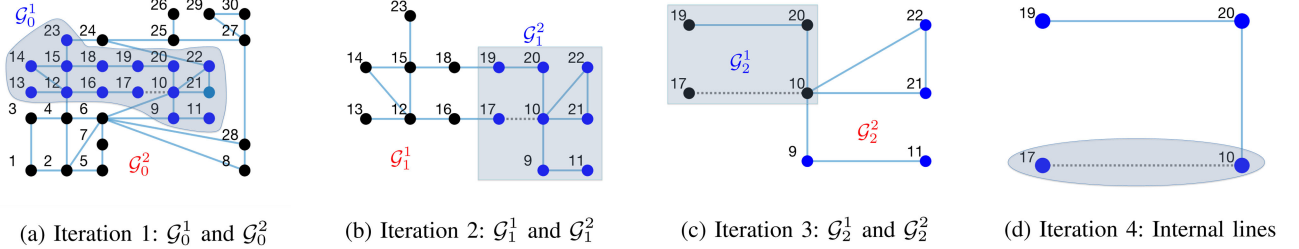


Fig. 7. Successively bisecting  $\mathcal{G}$  when  $E_{10,17}$  is in outage.

in parallel while following the maximum likelihood localization decision rule given by

$$\tau^{uv,ab} \triangleq \inf\{n \geq \hat{\gamma} : \max_{(u,v),(a,b) \in E} W^{uv,ab}[n] > C^{uv,ab}\}. \quad (35)$$

However, we note that in order to leverage our framework, i.e. to employ binary search to circumvent combinatorial complexity, we require that line outages either occur within a cluster of internal lines or be a tie-line connecting two clusters of internal lines. We note that this is to ensure that the bisection search (Algorithm-2) carried out in parallel for the two partitions consists of post-change models associated with their respective partitions. This, as a result, guarantees with high probability, that the W-CuSum statistic  $W_i^r[n] \forall r \in \{1, 2\}$  given by

$$W_i^r[n] \triangleq \left( W_i^r[n-1] + \log \left( \frac{g(\mathcal{S}_n(\mathcal{G}_i^r))}{f_i^r(\mathcal{S}_n(\mathcal{G}_i^r))} \right) \right)^+ \quad (36)$$

corresponding to either subgraphs satisfy the decision rule  $\tau_i^r$  given by

$$\tau_i^r \triangleq \inf\{n \geq \hat{\gamma} : W_i^r[n] > C_i^r\} \quad (37)$$

for the following modified mixture distribution

$$g(\mathcal{S}_n(\mathcal{G}_i^r)) = \sum_{(u,v),(a,b) \in E_i^r} \epsilon_{uv,ab}^r \cdot g_{uv,ab}^r(\mathcal{S}_n(\mathcal{G}_i^r)). \quad (38)$$

Therefore, when performed recursively, the search space reduces drastically every iteration circumventing the need for  $\binom{L}{2}$  parallel tests. In order detect and localize tie-line outages, there exist two possible double-line outage scenarios: (i) two tie-lines undergo an outage, and (ii) one tie-line and one internal line undergo an outage. In order to address (i), the statistic in (34) for all possible two tie-line combinations, for that iteration, are run in parallel with (36). To address (ii), we ensure that the mixture distribution in (38) includes post-change models that incorporates outages that share an edge with the tie-lines on either side of the two partitions in that specific iteration. As a result, for any given iteration that consists of  $T$  tie-lines, our approach requires  $2 + \binom{T}{2}$  test statistics in parallel as opposed to  $\binom{L}{2}$  test statistics. Therefore, when the lines are localized to a cluster of size 4 or fewer, the statistic in (34) can be employed to uniquely localize the double line outage via the decision rule in (35).

For simulations, we consider the 30-bus system in which we consider double-line outages that occur in close neighborhood to show the efficacy of the proposed approach. Specifically, we

TABLE VI  
PERFORMANCE OF DOUBLE LINE OUTAGE LOCALIZATION ALGORITHM  
(30-BUS)

MTF (Samples)	1,000	1,600	2,600	3,600
Line (10,20) and (10,17) outage				
LEP	0.09	0.09	0.04	0.032
ADD (sec)	0.047	0.051	0.057	0.061
ALD (sec)	0.081	0.083	0.087	0.091
Line (1,3) and (3,4) outage				
LEP	0.10	0.096	0.09	0.03
ADD (sec)	0.011	0.013	0.015	0.016
ALD (sec)	0.271	0.282	0.287	0.295
Line (4,12) and (4,6) outage				
LEP	0.12	0.09	0.076	0.063
ADD (sec)	0.029	0.030	0.032	0.035
ALD (sec)	0.126	0.131	0.134	0.142

consider three double-line outage cases: (i) lines (10,20) and (10,17) outage, (ii) lines (1,3) and (3,4) outage, and (iii) lines (4,12) and (4,6). In scenario (i) and (ii), we consider double-line outages of internal lines while for scenario (iii) we consider the outage of a tie-line and an internal line, as can be verified from Fig. 7(a). In Table VI, the LEPs take into account for realizations in which the true double line outage were not reported. The ADD and ALD denote the average delay to detection and localize the double-line outage. We observe that the delays and error probabilities are reasonable, as desired.

#### G. Line Outage Detection With a Subset of Measurements

Taking into consideration the deployment cost of PMUs and other inevitable concerns, it is not uncommon to have a partially observable network in which only a subset of buses  $\mathcal{O} \subset V$  are monitored. We extend our framework for outage detection under partially observable settings while providing an overview on how outage localization can be addressed. To address outage detection, we exploit the smooth and low-rank structure of real-time phasor measurements in order to reconstruct the graph signal  $\theta[n]$  from a subset of measurements which we denote by  $[\theta[n]]_{\mathcal{O}}$ . A consequence of such a structure in  $\theta[n]$  is that the graph frequency content, captured via the Graph Fourier Transform (GFT), of the graph signal  $\theta[n]$  resembles a low-pass filter characteristic rendering the signal spatially band-limited [31]. Therefore, graph signal transformations between the temporal and spatial domains results in approximately

TABLE VII  
PERFORMANCE OF ALGORITHM-3 UNDER 60% OBSERVABILITY (30-BUS)

MTF (Samples)	1,000	1,600	2,600	3,600
Line (4,12) outage				
ADD (sec)	0.083	0.085	0.098	0.14
MDP	0.06	0.08	0.13	0.15
LEP ( $m = 3$ )	0.34	0.34	0.29	0.28
Line (6,9) outage				
ADD (sec)	0.091	0.096	0.12	0.15
MDP	0.08	0.08	0.11	0.10
LEP ( $m = 3$ )	0.30	0.31	0.29	0.29
Line (22,24) outage				
ADD (sec)	0.089	0.098	0.13	0.16
MDP	0.03	0.11	0.13	0.13
LEP ( $m = 3$ )	0.23	0.21	0.17	0.12

lossless reconstruction errors. We leverage this property in our formulation discussed next.

Typically such transformations require an orthogonal basis which we obtain via the spectral decomposition of  $\mathcal{L}_B$  as follows:

$$\mathcal{L}_B = \mathbf{U} \cdot \boldsymbol{\Lambda} \cdot \mathbf{U}^\top \quad (39)$$

where  $\boldsymbol{\Lambda}$  is a diagonal matrix consisting of eigenvalues representing the graph frequencies  $\lambda_k$  for  $k \in [0, \dots, N-1]$ , ordered  $\lambda_0 = 0 \leq \lambda_1 \leq \dots \leq \lambda_{N-1}$ , on its principal diagonal and  $\mathbf{U}$  consists of eigenvectors associated with  $\lambda_k$  as column vectors. Hence, projecting the graph signal  $\boldsymbol{\theta}[n]$  onto the  $\mathcal{K}$  dominant eigen-basis results in an approximately lossless transformation. The observed measurements can alternately be represented by  $[\boldsymbol{\theta}[n]]_{\mathcal{O}} = P_{\mathcal{O}}^\top \cdot \boldsymbol{\theta}[n]$  where  $P_{\mathcal{O}} \in \mathbb{R}^{N \times N_{\mathcal{O}}}$  consists of coordinate vectors as columns such that it chooses a bus that is observed. As the GFT of  $\boldsymbol{\theta}[n]$  is given by  $\tilde{\boldsymbol{\theta}}[n] \triangleq \mathbf{U}_{\mathcal{K}}^\top \cdot \boldsymbol{\theta}[n]$ , the observed measurements satisfy

$$[\boldsymbol{\theta}[n]]_{\mathcal{O}} \approx P_{\mathcal{O}}^\top \cdot \mathbf{U}_{\mathcal{K}} \cdot \tilde{\boldsymbol{\theta}}[n] \quad (40)$$

where  $\mathbf{U}_{\mathcal{K}}$  denotes the eigenvectors corresponding to the first  $\mathcal{K}$  dominant graph frequencies. Following (40), the reconstructed graph signal  $\hat{\boldsymbol{\theta}}[n]$  is given by

$$\hat{\boldsymbol{\theta}}[n] = \mathbf{U}_{\mathcal{K}} \cdot (P_{\mathcal{O}}^\top \cdot \mathbf{U}_{\mathcal{K}})^\dagger \cdot [\boldsymbol{\theta}[n]]_{\mathcal{O}}. \quad (41)$$

Subsequently, the reconstructed measurements  $\hat{\boldsymbol{\theta}}[n]$  can be further employed by Algorithm-3 every iteration. We note that the necessary condition for reconstruction is that  $|\mathcal{O}| \geq |\mathcal{K}|$  as investigated in [32].

We consider the 30-bus system for our case study with 60% observability (18 PMUs monitored). The PMU locations are selected such that there exists atleast two PMUs in each 4-bus cluster. This is done so that the pdfs associated with each subgraph  $G_i^r$  closely approximates the true pdf of the subgraph, with errors induced due insufficient coverage. The pdfs associated with pre- and post-change smoothness metrics are re-estimated by running multiple power flows, this time employing the reconstructed measurements  $\hat{\boldsymbol{\theta}}[n]$ . In case of detection, Table VII tabulates the ADD and miss detection probability (MDP) for various MTFAs, where MDPs capture the number of realizations for which the

TABLE VIII  
EFFECT OF MODEL MISMATCH ON FAP FOR A MTFA = 1000 SAMPLES IN THE 30-BUS SYSTEM

$\frac{\sigma_1^2}{\sigma_0^2} \times 100$	-50%–0%	5%	10%	20%	50%
Line (4,12) outage					
FAP	$\frac{0}{1000}$	$\frac{10}{1000}$	$\frac{21}{1000}$	$\frac{112}{1000}$	$\frac{879}{1000}$
Line (6,9) outage					
FAP	$\frac{0}{1000}$	$\frac{10}{1000}$	$\frac{23}{1000}$	$\frac{132}{1000}$	$\frac{871}{1000}$
Line (22,24) outage					
FAP	$\frac{0}{1000}$	$\frac{10}{1000}$	$\frac{12}{1000}$	$\frac{84}{1000}$	$\frac{859}{1000}$

detection statistic  $W_d[n]$  failed to declare an outage. We note that in the previous case studies, the MDPs were negligible and therefore, we did not include MDP as part of the performance measure. However, since  $\hat{\boldsymbol{\theta}}[n]$  is only an approximation of  $\boldsymbol{\theta}[n]$  we observed a higher MDP for this case study.

In case of outage localization, we note that due to the added uncertainty in the reconstructed sequence  $\{\hat{\boldsymbol{\theta}}[n]\}_{n \geq 1}$  owing to the lossy reconstruction, the test statistics associated with line outages other than the true line in outage are likely to satisfy (30). As a consequence, this significantly increases the LEPs. Therefore, we modify the decision rule (30) to instead maintain a ranked list of CuSum statistics consisting of the  $m$  smallest stopping times (where (30) pertains to  $m = 1$ ). In this case, the LEPs denotes the probability of finding the true line in outage within the  $m$  smallest stopping times. We note that while this is not perfect localization, following such an approach can eliminate other candidate line outages with high probability. To localize the true line in outage, further tests can then be applied on the remaining lines, a topic of future work. Table VII summarizes the LEPs for the three single line outage cases.

#### H. Line Outage Detection and Identification Under Model-Mismatch

In practice, it is often difficult to estimate the true parameter  $\sigma_0$  with 100% accuracy. In this regard, we test our algorithm when there exists a model-mismatch between the true model and the assumed model for  $\Delta P$ , which subsequently induces a mismatch in  $\Delta \theta$ . In particular, when the assumed model for the fluctuations is given by  $\Delta P \sim \mathcal{N}(0, \sigma_1^2 \mathbf{I})$ , from (3) we observe that both the pre- and post-change models for  $\Delta \theta$  alters. Therefore, the pdfs  $f, f_{uv}$  (from Section III-B) alter and subsequently, the pdfs associated with the local and global smoothness metrics change. We denote the modified pdfs, parameterized by  $\sigma_1$ , by  $\tilde{f}, \tilde{f}_{uv}, \tilde{g}$  and  $\tilde{f}_i^r$  under the assumed model.

We consider a case study that empirically analyzes the effect of varying  $\sigma_1$  with respect to  $\sigma_0$ . Specifically, we consider the 30-bus system for which  $\sigma_0^2 = 0.5$  and vary  $\sigma_1^2$  over a broad range, i.e., from  $\{-50\%–50\%\} \cdot \sigma_0^2$ . In the experiments, we fix the MTFA = 1000 samples and run a Monte-Carlo over 1000 realizations to calculate the average detection and localization delay. In addition, we introduce a new figure of merit, i.e., the False Alarm Probability (FAP) that keeps track of the number of realizations for which an outage is declared prior to the true change point  $\gamma = 100$ . Figure 8 and Table VIII illustrates the effect of varying  $\sigma_1^2$  relative to  $\sigma_0^2$ . We observe that decreasing

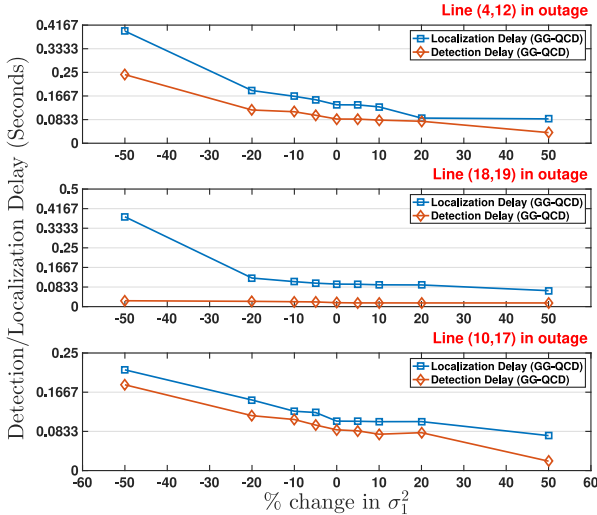


Fig. 8. Effect of model mismatch on average detection and localization delay for a MTFA = 1000 samples in the 30-bus system.

$\sigma_1^2$  increases the average delay while making it robust to FAP while increasing  $\sigma_1^2$  decreases the average delay at the expense of increasing the FAP.

## VII. CONCLUSION

In this paper, we have considered the problem of scalable and real-time detection and localization of transmission line outages. A low-complexity and scalable algorithm is designed by exploiting the global and local smoothness properties of phasor measurement data. Specifically, we have proposed a data-driven spectral graph-theoretic approach for testing the conformity of the data to the network structure. Designing change-detection tests based on these metrics has resulted in a significant reduction in the number of tests and the associated complexity for each test. The proposed framework is agnostic to the distribution of fluctuations in real-power injections and can also be further extended for detection and identification of multiple line outages without having to suffer from combinatorial complexity. Performance gains of the proposed approach have been compared against the existing approaches in the standard IEEE 30- and 118-bus systems.

## REFERENCES

- [1] "Aug. 14, 2003 blackout: NERC actions to prevent and mitigate the impacts of future cascading blackouts," Feb. 2014, [Online]. Available: [https://www.nerc.com/docs/docs/blackout/NERC\\_Final\\_Blackout\\_Report\\_07\\_13\\_04.pdf](https://www.nerc.com/docs/docs/blackout/NERC_Final_Blackout_Report_07_13_04.pdf)
- [2] J. E. Tate and T. J. Overbye, "Line outage detection using phasor angle measurements," *IEEE Trans. Power Syst.*, vol. 23, no. 4, pp. 1644–1652, Oct. 2008.
- [3] J. E. Tate and T. J. Overbye, "Double line outage detection using phasor angle measurements," in *Proc. IEEE Power Energy Soc. Gen. Meeting*, Calgary, Canada, Jul. 2009, pp. 1–5..
- [4] M. He and J. Zhang, "A dependency graph approach for fault detection and localization towards secure smart grid," *IEEE Trans. Smart Grid*, vol. 2, no. 2, pp. 342–351, May 2011.
- [5] J. Heydari and A. Tajer, "A graphical approach to quickest outage localization in power grids," in *Proc. IEEE Stat. Signal Process. Workshop*, Palma de Mallorca, Spain, Aug. 2016.
- [6] J. Heydari and A. Tajer, "Quickest localization of anomalies in power grids: A stochastic graphical framework," *IEEE Trans. Smart Grid*, vol. 9, no. 5, pp. 4679–4688, Sep. 2018.
- [7] J. Chen, Y. Zhao, A. Goldsmith, and H. V. Poor, "Line outage detection in power transmission networks via message passing Algorithms," in *Proc. Asilomar Conf. Signals, Syst. Comput.*, Pacific Grove, CA, Apr. 2014.
- [8] H. Zhu and G. B. Giannakis, "Sparse overcomplete representations for efficient identification of power line outages," *IEEE Trans. Power Syst.*, vol. 27, no. 4, pp. 2215–2224, May 2012.
- [9] J. Chen, W. Li, C. Wen, J. Teng, and P. Ting, "Efficient identification method for power line outages in the smart power grid," *IEEE Trans. Power Syst.*, vol. 29, no. 4, pp. 1788–1800, Jan. 2014.
- [10] R. Emami and A. Abur, "External system line outage identification using phasor measurement units," *IEEE Trans. Power Syst.*, vol. 28, no. 2, pp. 1035–1040, Oct. 2013.
- [11] T. Kim and S. J. Wright, "PMU placement for line outage identification via multinomial logistic regression," *IEEE Trans. Smart Grid*, vol. 9, no. 1, pp. 122–131, Mar. 2018.
- [12] Y. Zhao, J. Chen, and H. V. Poor, "Learning to infer: A new variational inference approach for power grid topology identification," in *Proc. IEEE Stat. Signal Process. Workshop*, Palma de Mallorca, Spain, Jun. 2016.
- [13] R. A. Sevlian, Y. Zhao, R. Rajagopal, A. Goldsmith, and H. V. Poor, "Outage detection using load and line flow measurements in power distribution systems," *IEEE Trans. Power Syst.*, vol. 33, no. 2, pp. 2053–2069, Jul. 2018.
- [14] Y. C. Chen, T. Banerjee, A. D. Domínguez-García, and V. V. Veeravalli, "Quickest line outage detection and identification," *IEEE Trans. Power Syst.*, vol. 31, no. 1, pp. 749–758, Feb. 2016.
- [15] G. Rovatsos, X. Jiang, A. D. Domínguez-García, and V. V. Veeravalli, "Statistical power system line outage detection under transient dynamics," *IEEE Trans. Signal Process.*, vol. 65, no. 11, pp. 2787–2797, Feb. 2017.
- [16] X. Yang, N. Chen, and C. Zhai, "A control chart approach to power system line outage detection under transient dynamics," *IEEE Trans. Power Syst.*, vol. 36, no. 1, pp. 127–135, Jan. 2021.
- [17] H. V. Poor and O. Hadjiliadis, *Quickest Detection*. Cambridge, U.K.: Cambridge Univ. Press, 2008.
- [18] Y. Liao, Y. Weng, C.-W. Tan, and R. Rajagopal, "Fast distribution grid line outage identification with μPMU," 2018, *arXiv:1811.05646*.
- [19] L. Chen, S. Li, and X. Wang, "Quickest fault detection in photovoltaic systems," *IEEE Trans. Smart Grid*, vol. 9, no. 3, pp. 1835–1847, Aug. 2018.
- [20] D. Kunisky, S. A. Wein, and A. S. Bandeira, "Notes on computational hardness of hypothesis testing: Predictions using the low-degree likelihood ratio," 2019, *arXiv:1907.11636v1*.
- [21] D. I. Shuman, S. K. Narang, P. Frossard, A. Ortega, and P. Vandergheynst, "The emerging field of signal processing on graphs: Extending high-dimensional data analysis to networks and other irregular domains," *IEEE Signal Process. Mag.*, vol. 30, no. 3, pp. 83–98, Apr. 2013.
- [22] A. Ortega, P. Frossard, J. Kováčević, J. M. F. Moura, and P. Vandergheynst, "Graph signal processing: Overview, challenges, and applications," *Proc. IEEE*, vol. 106, no. 5, pp. 808–828, Apr. 2018.
- [23] M. Pollak, "Optimal detection of a change in distribution," *Ann. Statist.*, vol. 13, no. 1, pp. 206–227, Apr. 1985.
- [24] D. S. Matteson and N. A. James, "A nonparametric approach for multiple change point analysis of multivariate data," *J. Amer. Stat. Assoc.*, vol. 109, no. 505, pp. 334–345, Nov. 2014.
- [25] D. A. Stephens, "Bayesian retrospective multiple-changepoint identification," *J. Roy. Stat. Soc. Ser. C. (Appl. Statist.)*, vol. 43, no. 1, pp. 159–178, Sep. 1994.
- [26] G. V. Moustakides, G. H. Jajamovich, A. Tajer, and X. Wang, "Joint detection and estimation: Optimum tests and applications," *IEEE Trans. Inf. Theory*, vol. 58, no. 7, pp. 4215–4229, Jan. 2012.
- [27] A. Vexler and C. Wu, "An optimal retrospective change point detection policy," *Scand. J. Statist.*, vol. 36, no. 3, pp. 542–558, Sep. 2009.
- [28] A. Pothen, H. D. Simon, and K.-P. Liou, "Partitioning sparse matrices with eigenvectors of graphs," *SIAM J. Matrix Anal. Appl.*, vol. 11, no. 3, pp. 430–452, Jul. 1990.
- [29] T. F. Chan, P. Ciarlet, and W. K. Szeto, "On the optimality of the median cut spectral bisection graph partitioning method," *SIAM J. Sci. Comput.*, vol. 18, pp. 943–948, May 1997.
- [30] R. D. Zimmerman, C. E. Murillo-Sánchez, and R. J. Thomas, "MATPOWER: Steady-state operations, planning, and analysis tools for power systems research and education," *IEEE Trans. Power Syst.*, vol. 26, no. 1, pp. 12–19, Jun. 2011.
- [31] R. Ramakrishna and A. Scaglione, "Grid-graph signal processing (grid-GSP): A graph signal processing framework for the power grid," 2021, *arXiv:2103.06068v1*.
- [32] M. Tsitsvero, S. Barbarossa, and P. Di Lorenzo, "Signals on graphs: Uncertainty principle and sampling," *IEEE Trans. Signal Process.*, vol. 64, no. 18, pp. 4845–4860, May 2016.